



HAL
open science

What is happening around the KVLCC2?

Jeroen Wackers, Ganbo Deng, Emmanuel Guilmineau, Alban Leroyer, Patrick Queutey, Michel Visonneau

► To cite this version:

Jeroen Wackers, Ganbo Deng, Emmanuel Guilmineau, Alban Leroyer, Patrick Queutey, et al.. What is happening around the KVLCC2?. 18th Numerical Towing Tank Symposium (NuTTS 2015), Sep 2015, Cortona, Italy. hal-01202593

HAL Id: hal-01202593

<https://hal.science/hal-01202593>

Submitted on 26 Oct 2020

HAL is a multi-disciplinary open access archive for the deposit and dissemination of scientific research documents, whether they are published or not. The documents may come from teaching and research institutions in France or abroad, or from public or private research centers.

L'archive ouverte pluridisciplinaire **HAL**, est destinée au dépôt et à la diffusion de documents scientifiques de niveau recherche, publiés ou non, émanant des établissements d'enseignement et de recherche français ou étrangers, des laboratoires publics ou privés.



Distributed under a Creative Commons Attribution 4.0 International License

What is happening around the KVLCC2?

Jeroen Wackers, Ganbo Deng, Emmanuel Guilmineau,
Alban Leroyer, Patrick Queutey, and Michel Visonneau
LHEEA, Ecole Centrale de Nantes / CNRS-UMR 6598, 1 rue de la Noë, Nantes, France
Jeroen.Wackers@ec-nantes.fr

1 Introduction

The flow around the well-known KRISO Very Large Crude Carrier no. 2 (KVLCC2) is characterised by boundary layer thickening, flow separation, and vortex creation on the aft body of the ship, leading to a very non-homogeneous velocity field in the propeller plane (figure 1). It is known since the 1990s that the numerical simulation of such flows is highly sensitive to the treatment of the turbulence. For RANS equations, standard turbulence models perform poorly; measures like the anisotropic treatment of turbulence production are necessary in order to compute correctly the most famous aspect of the flow, the hook-shaped low-velocity zone in the main longitudinal vortex. The case is therefore justly famous as a test of turbulence models for marine flow simulation.

The focus of most studies that use the KVLCC2, such as Larsson et al. [3], is the comparison of different flow solvers or different turbulence models. To keep such studies compact and accessible, comparisons are mostly done for a few physical features only. The propeller plane with its hook shape in the axial velocity is often studied.

The objective of this paper, on the contrary, is to use a single numerical simulation of good quality to visualise the entire flow field around the aft body of the KVLCC2. We then attempt a physical analysis of this flow, searching explanations of less-studied features such as the outer boundary layer shape and the flow behind the propeller hub cap. We hope that better knowledge of the flow will allow, in the future, to understand more precisely the behaviour of different turbulence models, which may ultimately lead to better models.

The paper starts with a definition of the test case and the computation (section 2). Then section 3 presents the visualisation and analysis of the numerical solution. To assess the validity of the analysis, selected aspects of the solution are compared with experiments in section 4. The conclusion (section 5) addresses the challenges for turbulence modelling which the KVLCC2 test case still presents.

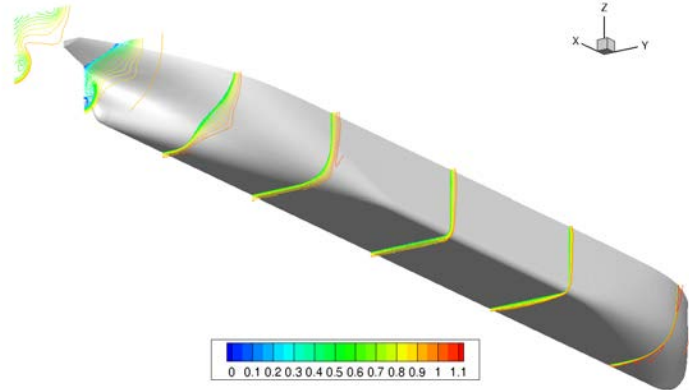


Figure 1: KVLCC2 geometry and cuts of the axial velocity.

2 Test case and numerical simulation

The case considered is the double-model flow around the KVLCC2 tanker in straight-ahead motion. The Reynolds number is $Re = 4.6 \cdot 10^6$. We compare velocities and turbulent quantities with windtunnel measurements performed at Postech [4]. The computation is performed with the ISIS-CFD flow solver [5]; it is part of a systematic grid refinement study, using automatic mesh adaptation [6]. The turbulence is modelled with the anisotropic EASM turbulence closure [1].

Half the ship is simulated. The domain runs from $4L$ in front of the bow to $9L$ behind the stern, where L is the length between perpendiculars. Sidewards and downwards, it has a size of $4L$. Boundary conditions are symmetry on the two sides of the domain which touch the hull, imposed velocity on the inflow face and the two other sides, and imposed pressure on the outflow. The hull itself has a no-slip condition, for low-Reynolds simulation of the boundary layers. The initial grids for the adaptive refinement are made with the HEXPRESSTM grid generator from NUMECA Int. The target y^+ for the first cells on the hull is 0.3, which gives 25 layers in the boundary layer grid.

Grid adaptation is performed with the flux-component Hessian criterion [7] which assures good resolution of the wake. A refinement threshold of $T_r = 1.5$ gives a refined grid of $8M$ cells. The solution on this grid is close to grid-independent, as shown in figure 2: solutions on coarser grids created with larger thresholds have a local flow which is nearly identical.

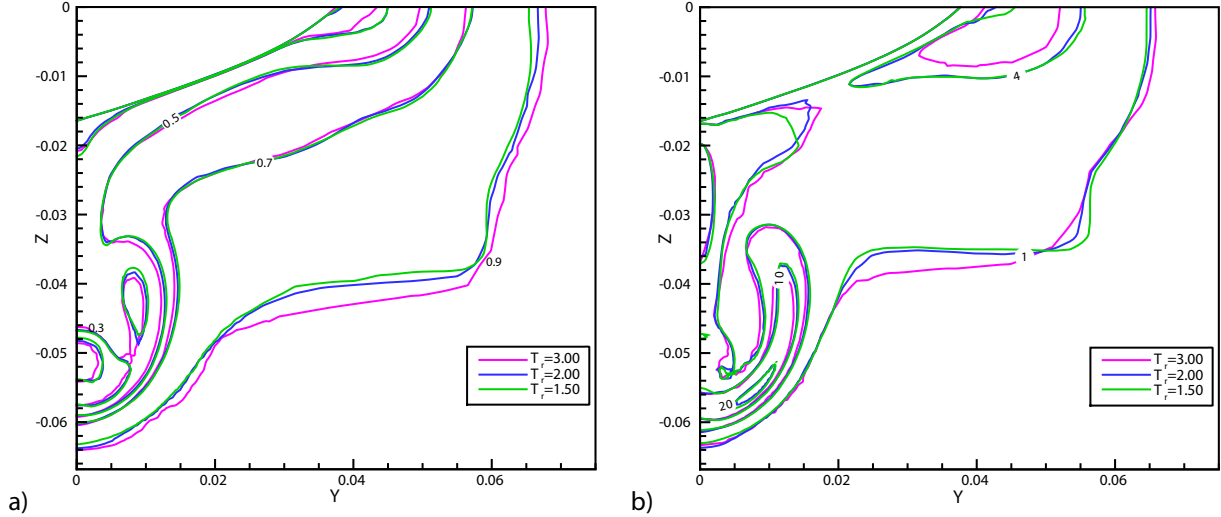


Figure 2: Grid convergence study of the axial velocity (a) and turbulence kinetic energy (b) in the propeller plane.

3 Flow analysis

Here, we identify the different phenomena in the flow simulated as in section 2, and analyse them one by one.

3.1 Visualisation

Figure 3 shows both the mean flow and the turbulence around the aft body; figure 4 gives a more detailed view of the bulb surrounding the propeller shaft and the hub cap. The mean velocity is represented by the axial velocity u and the vertical velocity w , which plays an important role in the formation of the hook shape. Vortical structures are identified with an isosurface of the second invariant Q of the velocity gradient, coloured with the helicity to show the direction of rotation. Wall and symmetry-plane streamlines complete the mean-flow visualisation.

The turbulence intensity is characterised by the turbulence kinetic energy k . To study the level of anisotropy in the turbulence, we consider that $k = \frac{1}{2}(\overline{u'u'} + \overline{v'v'} + \overline{w'w'})$, so in isotropic turbulence $\overline{u'u'} = \frac{2}{3}k$. Thus, $\overline{u'u'}/k - \frac{2}{3}$ is an indicator of anisotropy; whenever this parameter is positive, the turbulence is dominated by axial velocity fluctuations. The near-wall turbulent boundary layer is represented by the wall shear stress. Also, the amount of twist in the boundary layer is assessed by showing the wall-normal derivative of the velocity vector angle, i.e. the angle between the velocity vectors in the first and second cells next to the wall, divided by the cell-centre distance. Ideally, the twist is determined by comparing the near-wall flow direction with the angle of the flow outside the boundary layer, but the KVLCC2 aft-body boundary layer is so thick that this makes little sense: the entire aft-body flow is technically in the boundary layer!

3.2 Shoulder vorticity regions (USVR, LSVR)

The development of the KVLCC2 aft-body wake starts with the appearance of two vortical regions in the boundary layer, on the ‘shoulders’ where the flat side wall and bottom start to curve inwards; these regions are labelled USVR and LSVR, for Upper and Lower Shoulder Vorticity Region, respectively (figure 3c). The flow does not separate here, as confirmed by the non-zero wall shear stress (figure 3g, mark A), so the USVR and LSVR are not free vortices. However, they have a sense of rotation, shown by opposite and non-zero values of the helicity. As a result, they induce cross-flows which compress the boundary layer towards the centre of the inward-curving wall. There, the boundary layer thickens rapidly and forms a pointy shape where the converging cross-flows meet (figure 3a, B).

While the LSVR and USVR are pressure-driven features which do not depend much on the turbulence, they have a strong influence on the turbulent boundary layer. Figure 3b, C indicates that the cross-flow is zero on the wall and increases to a maximum in the centre of the boundary layer. Thus, the fluid which is displaced is mainly the high-velocity, low-turbulence fluid of the outer boundary layer. Therefore, the turbulence level in the cross-flow region (figure 3e, D) is lower than in the boundary layers on the horizontal and vertical walls (E). The anisotropy of the turbulence, seen in figure 3f, is (surprisingly!) high in the non-disturbed boundary layers on the walls (F). Where the cross-flows meet, the turbulence becomes isotropic (G). Thus, the nature of the turbulence changes; the simple convection of low-turbulence fluid to the cross-flow region may therefore not be the only explanation of the low k in this region.

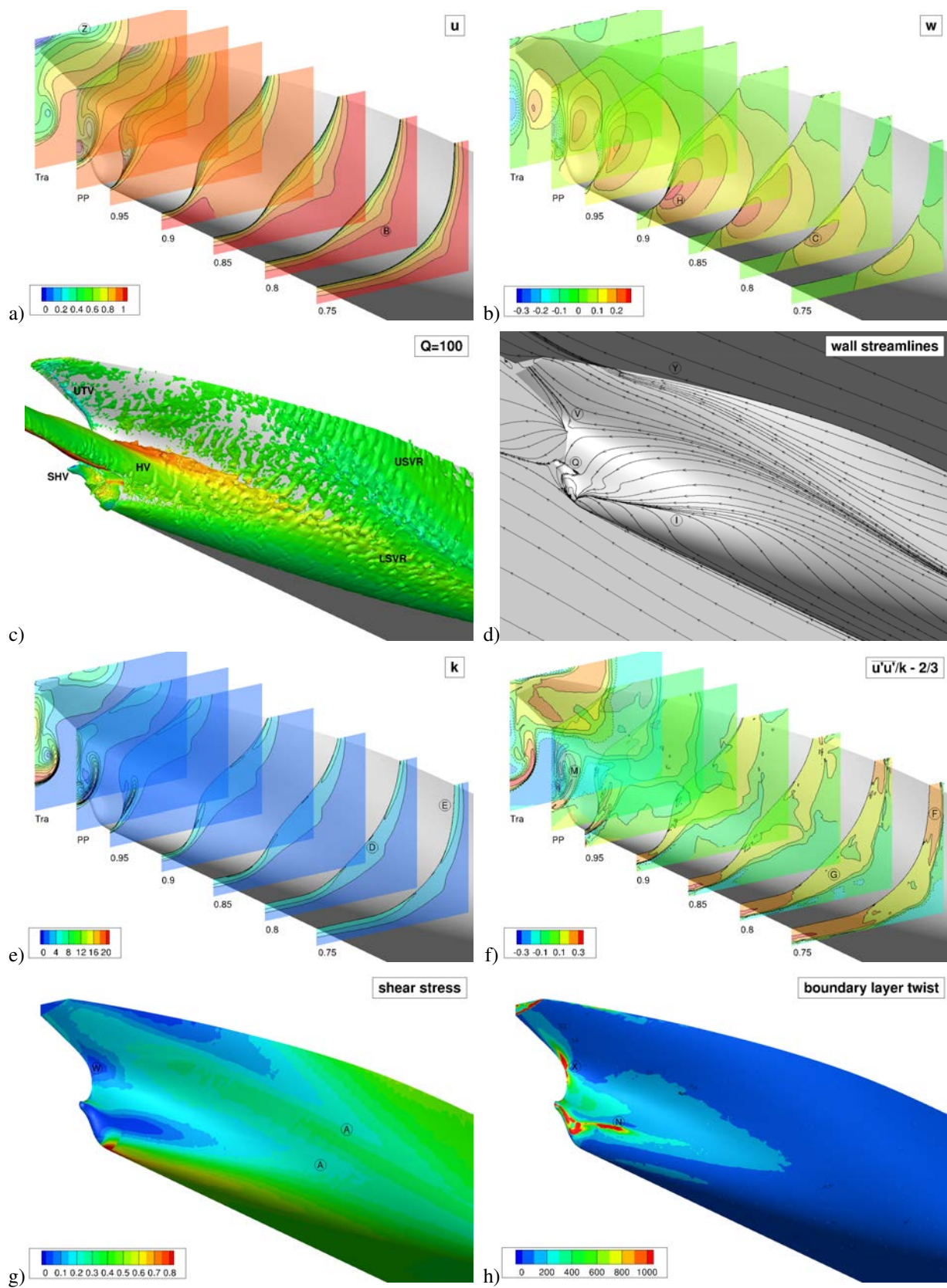


Figure 3: Visualisation of the flow on the aft part of the hull. The marks (A, B, etc.) are referenced in the text.

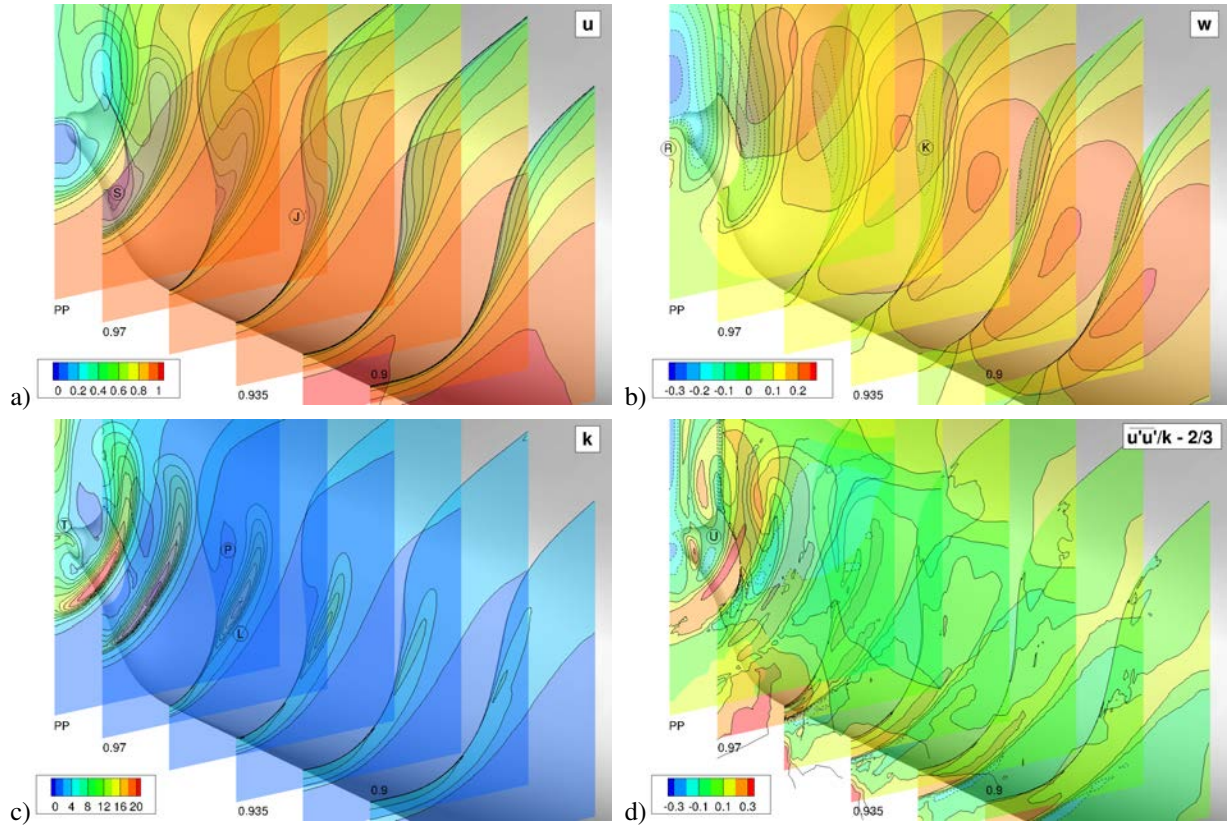


Figure 4: Visualisation of the flow on the aft part of the hull (detail of figure 3).

3.3 Hook vortex (HV)

Further back, the flow induced by the LSVR moves upwards along the hull. When this updraft flows around the bulb which surrounds the propeller axis (figure 3b, *H*), an open-type separation appears which forms the main Hook Vortex (HV), see figures 3c and d, *I*. The separation is comparable to the vortex shedding on an ogive at an angle of incidence. The core of the HV originates in the near-wall boundary layer and therefore has a low axial velocity (figure 4a, *J*). This core, and the shear layer below which connects it to the boundary layer, form the hook shape of low axial velocity which is the best-known feature of this test case. The vortex induces a downward flow on the hull (figure 4b, *K*), which gradually separates the vortex core from the hull.

Since the separation of the HV occurs on a smooth surface, it depends on the evolution of the turbulent boundary layer. And the separation line is precisely the location of the most violent turbulence production in the entire flow (figure 4c, *L*), caused by the shear in the axial velocity between the fast outer flow and the dead-water region of separated fluid. The shear in the vertical velocity is much less marked. This shear-layer turbulence, like the boundary layers, is anisotropic and dominated by axial fluctuations (figure 3f, *M*). Also, the near-wall boundary layer is strongly twisted (figure 3h, *N*).

On the contrary, the core of the HV where u is the lowest is a region of very low turbulent kinetic energy (figure 4d, *P*). A possible explanation is, that the low-velocity fluid comes from the inner part of the boundary layer which is compressed by the downward flow on the hull; this fluid close to the wall has a low k . However, the vortex core area is large compared with the very thin inner boundary layer, so an additional damping phenomenon may exist. Since the core evolves in a zone of low turbulence, it persists over a long distance.

3.4 Secondary hook vortex (SHV)

The downward velocity on the hull, induced by the HV, starts above the shaft bulb but rapidly flows around the bulb and pushes the separation point of the HV downwards (see figures 4a, *J* and 3d, *I*). Below the bulb, the downward flow separates in its turn (figure 3d, *Q*). This separated flow encounters an updraft which follows the lower part of the bulb upwards (figure 4b, *R*). Between them, these flows create the Secondary Hook Vortex (SHV), which is counter-rotating with respect to the HV. The SHV separation resembles the ones on bluff bodies with oblique aft faces; there is a significant dead-water zone with low axial velocity between the vortex and the centre plane (figure 4a, *S*). This dead-water zone, clearly visible in the propeller plane, is therefore not the direct wake of the hub cap but it is created on the hull, below and in front of the hub cap.

Just above the dead-water region, the velocity gradients are high. There is some production of turbulence in this zone (figure 4c, T). The vortex core appears to be a minimum of k but it is not a zone of uniform anisotropy; predominance and relative absence of axial fluctuations appear side by side (figure 4d, U).

3.5 Other separations and vortices

The flow on the upper part of the hull continues without major perturbations and then separates suddenly on the meeting point between the skeg and the hull below the transom, just before arriving at the end of the hull (figure 3d, V). The resulting, very weak under-transom vortex (UTV) follows the hull upwards. While it remains close, it is separated from the hull as seen in the shear stress (figure 3g, W), which is zero only at the origin of the UTV. Like the HV and SHV, the origin of the UTV is a location of strong boundary layer twist (figure 3h, X). Otherwise, its influence on the flow is marginal.

A much more pronounced wake is formed by the flow leaving the hull at its top edge. While the shear stress in this zone is low, the streamlines indicate that the flow remains attached throughout and leaves the hull at the upper edge (figure 3d, Y). In the wake, there is a significant velocity defect (figure 3a, Z) and some turbulence production.

4 Comparison with experiments

The preceding study is performed on numerical results, because these provide excellent resolution of details throughout the flow and allow the study of quantities which cannot be obtained from experiments. However, these results are subject to modelling errors so they could lead to false conclusions. Therefore, selected quantities in the propeller plane are compared with the windtunnel measurements, to see if these support the analysis in section 3.

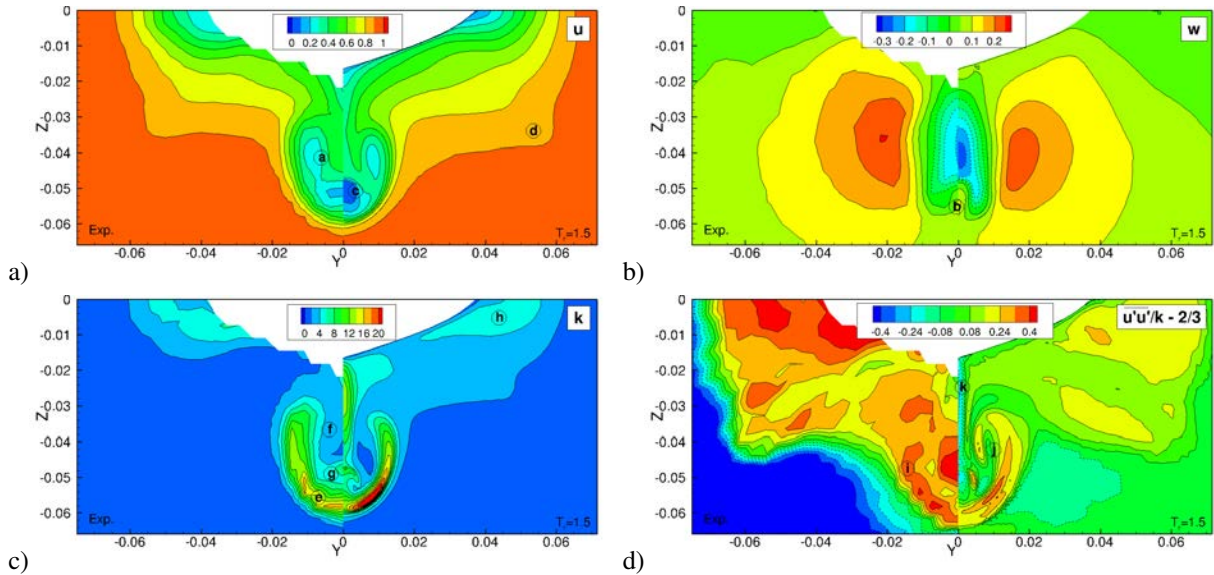


Figure 5: Comparisons of computational and experimental results in the propeller plane ($x = 0.9825L$).

The velocity measurements confirm the existence of the HV, SHV, and the USVR / LSVR. The hook shape, which is a characteristic of the HV, is very similar between computations and experiments (figure 5a, a). The downward jet and upward motion near the symmetry plane which form the SHV are present in the measurements (figure 5b, b). And while the axial velocity in the SHV core is higher in the experiments (figure 5a, c), this is not an error in the flow topology, since the vortex damps out so quickly: only $0.005L$ behind the propeller plane, the numerical solution has the same axial velocity as the experimental value in the propeller plane. Finally, the shape of the outer boundary layer edge (figure 5a, d) is due mainly to the USVR and LSVR; this shape is nearly identical between experiment and simulation, which supports the existence of these vorticity regions. The UTV is too weak and too close to the boundary to be seen in the experiments. Given the observed quality of the numerical solution, its existence is plausible, but it cannot be proved.

Figure 5c indicates that the prediction of the turbulence kinetic energy is also good. The high intensity in the HV shear layer (e), the low turbulence in the HV core (f), and the small peak of turbulence above the SHV (g) are confirmed, as is the slightly higher k besides the transom (h). The peak experimental value of k below the HV is not as high as in the simulation, but this may be due to the insufficient resolution of the measurements. Even the derived quantity of the anisotropy indicator (figure 5d) is mostly in good agreement, at least quantitatively. The predominance of longitudinal turbulence in the shear layers is confirmed (i); the isotropic turbulence in the HV core is not observed (j), but this may again be due to the insufficient resolution of the experiments.

Discrepancies are observed in the vertical symmetry plane (figure 5d, k , for example). However, the measurements are uncertain here, since the windtunnel results do not agree with towing tank measurements for the same geometry [3]. This area will be studied further in our future work.

5 Conclusion: challenges for turbulence modelling

The agreement between experiments and computations in the previous section is good, but not perfect. Due to the low numerical uncertainty (section 2) and supposing limited measurement errors, most differences can be attributed to the turbulence modelling. For these models, what can be learned from the physical analysis in section 3?

Traditionally, the challenge for simulating ships like the KVLCC2 with RANS has been the prediction of low enough turbulence in the HV core, so that this core is preserved intact. Standard turbulence models like $k - \omega$ SST produce too much turbulence viscosity near this core, so that it is damped out too quickly. Anisotropic models such as EASM produced the first simulations where the hook shape was predicted correctly.

This study shows that the driving force for the KVLCC2 aft-body flow, besides pressure effects, is boundary layer separation; thus, an additional challenge is to model these separations correctly. The separate flow regions have a very different nature:

- The flow in the USVR and LSVR remains attached, so it is within the validity region of classical RANS turbulence closures (even though the real turbulence is not at all isotropic!).
- The HV, with its axial-aligned separation line and relatively limited axial-velocity defect, is similar to the sonar dome vortex of the DTMB 5415 for which Larsson et al. [3] conclude that most RANS methods can predict the onset, given sufficiently fine grids. As noted above, the main difficulty is in preserving the low-velocity core. However, for any separation from a smooth surface, the simulated separation depends on the turbulence model, so there is a challenge here to get the separation line correct in order to predict the HV strength and position perfectly.
- The SHV separates from a surface that is not at all aligned with the main flow. Its separation, with a large low-velocity zone, resembles the one on a bluff body with an oblique aft part such as the Ahmed body (a simplified car geometry). Investigations have shown that today's RANS models are unable to predict this separation correctly; Detached-Eddy Simulation (DES) or similar techniques are required to better capture the flow, see for example [2]. By the way, this study finds that RANS overestimates the size of the recirculation zone, just like for the KVLCC2 (section 4). Thus, it remains to be seen whether RANS can ever simulate the SHV correctly.

The KVLCC2 results, confirmed by experiments, indicate that the turbulence is highly anisotropic and that the level of anisotropy depends on the position in the flow. This is not a proof that isotropic turbulence models perform badly for the KVLCC2. However, a turbulence model cannot duplicate the exact physics of the flow unless anisotropy is taken into account. Likewise, significant boundary layer twist was detected near separation zones. This could mean that wall-law boundary conditions, which use an approximated representation of the twist, may be unable to represent correctly the flow physics.

Thus, the KVLCC2 flow and especially the SHV is still a major challenge for turbulence modelling and the test case remains relevant for development work in the years to come.

Acknowledgements

This work is part of an ongoing collaboration with Alexandro Palmieri (CIRI-MAM Tecnopolo della Nautica, Università di Bologna, Italy). Computations were performed using HPC resources from GENCI (Grant2010-x2010021308), which is gratefully acknowledged.

References

- [1] R. Duvigneau, M. Visonneau, and G.B. Deng. On the role played by turbulence closures in hull shape optimization at model and full scale. *J Mar Sci Techn*, **8**(1), 1–25 (2003).
- [2] E. Guilmineau, G.B. Deng, and J. Wackers. Numerical simulation with a DES approach for automotive flows. *J Fluids Struct* **27**(5-6)807–816 (2011).
- [3] L. Larsson, F. Stern, and M. Visonneau (eds.). *Numerical Ship Hydrodynamics. An assessment of the Gothenburg 2010 workshop*. Springer (2013).
- [4] S.J. Lee, H.R. Kim, W.J. Kim, and S.H. Van. Wind tunnel tests on flow characteristics of the KRISO 3,600 TEU container ship and 300K VLCC double-deck ship models. *J Ship Res*, **47**(1), 24–38 (2003).
- [5] P. Queutey and M. Visonneau. An interface capturing method for free-surface hydrodynamic flows. *Comput Fluids*, **36**(9), 1481–1510 (2007).
- [6] J. Wackers, G.B. Deng, E. Guilmineau, A. Leroyer, P. Queutey, and M. Visonneau. Combined refinement criteria for anisotropic grid refinement in free-surface flow simulation. *Comput Fluids*, **92**, 209–222 (2014).
- [7] J. Wackers, E. Guilmineau, A. Palmieri, and P. Queutey. Hessian-based grid refinement for the simulation of surface-piercing hydrofoils. Proceedings of NuTTS 2014, Marstrand, Sweden (2014).